Pyrite with lower cubic symmetry from Lavrion, Greece
Pirit z nižjo kubično simetrijo iz Lavriona, Grčija

Mirjan ŽORŽ[1], Panagiotis VOUDOURIS[2] & Branko RIECK[3]

[1]Prešernova 53, SI-1290 Grosuplje, Slovenia; e-mail: zorz@siol.net
[2]National and Kapodistrian University of Athens, Faculty of Geology & Geoenvironment,
Department of Mineralogy and Petrology, University Campus-Zografou, 15784, Athens, Greece;
e-mail: voudouris@geol.uoa.gr
[3]Institut für Mineralogie und Kristallographie, Universität Wien, Althanstrasse 14, A-1090 Wien, Austria;
e-mail: rieckb49@univie.ac.at

Abstract

In this study, we examined the morphological, chemical, and structural details of tetrahedral pyrite crystals from the Jean Baptiste mine in Lavrion, Greece. Pyrite occurs in three generations. Tetrahedral crystals of the first generation are left- or right-handed with the lowest cubic *23* symmetry. In this generation, there are twins with higher cubic $m\overline{3}$ and hexagonal *6* symmetry. All crystals of the second generation are primarily interpenetrated into twins with a cubic $\overline{4}m3$ symmetry. Some, however, continue to twin up to crystals with the highest cubic $m\overline{3}m$ and hexagonal *6mm* symmetry. Third-generation crystals overgrow second-generation crystals in a non-oriented manner. Chemical analysis confirms chemically pure pyrite, and single-crystal X-ray analysis of the first- and the second-generation crystals confirms the pyrite-specific $m\overline{3}$ symmetry. The morphology of the single crystals and twins indicates that first generation of single pyrite crystals should have the lowest cubic *23* symmetry, which is not confirmed by the structural analysis. This discrepancy may be due to changed pT conditions and the consequent transformation of the original pyrite structure with symmetry *23* into a secondary structure with $m\overline{3}$ symmetry, or to suboptimal conditions in determining the structure by X-ray diffraction.

Izvleček

V tej študiji smo preučili morfološke, kemijske in strukturne podrobnosti tetraedrsko oblikovanih kristalov pirita iz rudnika Jean Baptiste v Lavrionu. Pirit se pojavlja v treh generacijah. Prvo predstavljajo tetraedrski levo oziroma desno sučni kristali z najnižjo kubično *23* simetrijo. V tej generaciji so dvojčki z višjo kubično $m\overline{3}$ in heksagonalno 6 simetrijo. Vsi kristali druge generacije so že primarno zdvojčeni do kubične $\overline{4}m3$ simetrije. Nekateri pa se dvojčijo še naprej dokler ne dosežejo najvišje kubične $m\overline{3}m$ ali heksagonalne *6mm* simetrije. Kristali tretje generacije neorientirano prekrivajo kristale druge generacije. Kemijska analiza potrjuje kemijsko čist pirit, monokristalna rentgenska analiza kristalov prve in druge generacije pa za pirit značilno $m\overline{3}$ simetrijo. Očitno je torej, da morfološke oblike posameznih kristalov in dvojčkov kažejo na to, da imajo najnižjo kubično simetrijo, česar pa strukturna analiza ne potrjuje. Ta diskrepanca je lahko posledica spremenjenih pT pogojev in posledične transformacije prvotne strukture pirita s simetrijo *23* v sekundarno strukturo z $m\overline{3}$ simetrijo ali pa neoptimalnih pogojev pri določitvi strukture z rentgensko difrakcijo.

Introduction

Lavrion ore district, located about 50 km southeast of Athens (Greece), is famous for exploitation of silver-rich lead ore during ancient times (Marinos & Petrascheck, 1956). The district includes two extensive mining centers, Plaka and Kamariza, as well as several smaller ones, covering an outcrop area of about 150 km^2 (Fig. 1a). The Lavrion mines were operated almost continuously from the 4th millennium BC until the Late Roman period, and then until late 20th century (Conophagos, 1980; Morin & Photiades, 2012). The Lavrion ore district hosts a carbonate-replacement Pb-Zn-Ag-Au deposit (Marinos &

Petraschek, 1956). It is well established that in addition to the carbonate-replacement style ores, four types of mineralization occur at Lavrion district: porphyry-type Mo-W ores in granodiorite, Cu-Fe-skarns, and Pb-Zn-Ag bearing breccias, and Pb-Zn-Ag-Au rich veins (Skarpelis, 2007; Voudouris et al., 2008; Bonsall et al., 2011; Scheffer et al., 2017, 2019). The ore deposits in Lavrion are structurally and lithologically controlled, and ore formation occurred under extensional kinematic conditions (Skarpelis, 2007; Berger et al., 2013; Scheffer et al., 2017, 2019).
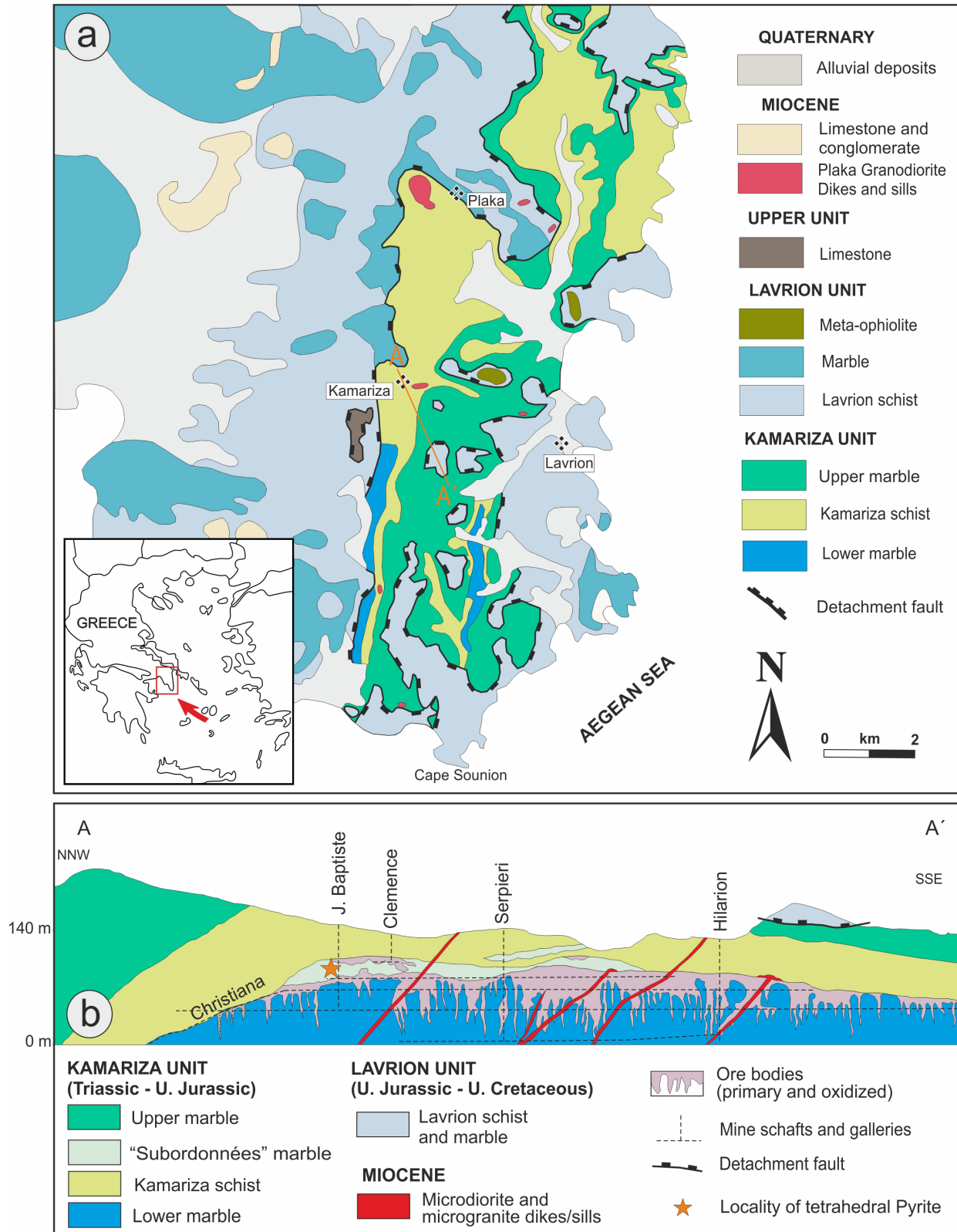
Fig. 1. (a) Simplified geological map of the Lavrion ore district (from Marinos and Petraschek 1956, Scheffer et al. 2016 and modified after Voudouris et al. 2021); (b) Cross-section A-A' of the Kamariza deposit (see geological map, figure 1a) (from Marinos and Petraschek 1956, modified after Voudouris et al. 2008).

Carbonate-replacement Pb-Zn-Ag±Au deposits at Kamariza are located in the central part of the district (Fig. 1a; Voudouris et al., 2008). The carbonate-replacement mineralization occurs in the form of stratabound massive sulfide replacement bodies (mantos) and chimneys, crosscutting with respect to layering in the host marble (Skarpelis, 2007; Voudouris et al., 2008; Bonsall et al., 2011, Scheffer et al., 2017 and 2019; Fig. 1b). Stratabound massive sulfide bodies (mantos) at Kamariza occur within the marbles as well as along the contacts of rocks with different permeabilities (marbles and schists). Ore deposition took place mainly from high-T magmatic fluids during the transitional ductile/brittle and brittle deformation stage of the host rocks (Bonsall et al., 2011; Scheffer et al., 2017, 2019). Beneath the individual manto orebodies, the rocks are cut by N-S to NE-SW, and NW-SE to E-W trending and steeply dipping veins that follow faults and fissures. The veins are usually zoned and brecciated, and in the breccias, the fragments are cemented by a sulfide-rich matrix. Pb-Zn-Ag veins are generally found below but also above the Lavrion detachment in the marbles of the Lavrion unit, in the Upper marble, in the Kamariza schists and at the interface between the Kamariza schists and the Lower marble. N-S trending veins crosscut the "Subordonnés" formation in the Jean Baptiste deposit (Fig. 1b). The veins are thought to be fluid pathways and feeder zones for the stratabound mineralization. The vein-style deposits were formed as the rock entered the brittle regime, by mixed seawater and meteoric fluids (Bonsall et al., 2011; Scheffer et al., 2017, 2019). The Jean Baptiste mine is located in the northwest area of the Kamariza district (Figs. 1a and b). Its mineralization consists of several vertical veins that have been the target of modern mining on the first level (and above) of the mine in the beginning of 20th century. The veins show ore zoning, whereby the crystallized minerals are present in the veins and in horizontal fissures. Tetrahedral pyrite crystals were found by chance in 2001 in a detached chamber within the Jean Baptiste mine that used to be a small ore prospection. It was obviously of no significant commercial value and consequently abandoned. Euhedral tetrahedral pyrite crystals grew within the banded marble and in the open ore veins hosting crystallized arsenopyrite, sphalerite, galena, calcite, dolomite, aragonite, and quartz.

Pyrite is the most widespread sulfide mineral that occurs in a wide range of morphological shapes. It comes in the form of single crystals belonging to cubic $m\overline{3}$ point group (symmetry further in text). The most frequent crystallographic forms are cube {100}, octahedron {111}, and pentagon dodecahedron, i.e. pyritohedron {210} that dictate the basic crystal morphology, which is further modified by many accessorial crystallographic forms. Distorted, i.e. elongated single pyrite crystals are common appearances. Their symmetry depends on elongation direction. If they are elongated in (111)- and (100)-direction they develop 3-fold form with morphologic $\overline{3}m$ symmetry and 2-fold form with morphologic mmm symmetry, respectively. All other orientations yield elongated crystals with 1-fold morphologic symmetry. Situation changes if the crystals are attached to a matrix. If they are attached with their [111]- and [110]-axis they develop chiral morphologic 3 and 2 symmetry, respectively. All other attachment possibilities result in chiral morphologic 1 symmetry, with a single exception of [001]-axis attachment that results in a non-chiral $mm2$ morphology (Žorž, 2019). Pyrite basic $m\overline{3}$ symmetry does not allow the existence of tetrahedral crystals. If this is the case then the octahedron {111} transforms either to positive t{111} or to negative $\overline{t}${$\overline{1}$11} tetrahedrons with the resulting lower cubic $\overline{4}m3$ or 23 symmetries. Morphologic distortion of octahedral crystal morphology that would lead to a predominance of four octahedron faces and consequently to a tetrahedral crystal shape is not known.

Pyrite is often associated with other minerals in epitactic, i.e. in oriented growth relationships. Of them, the most frequent is epitaxy of pyrite on marcasite and vice versa. Richards et al. (1995) reported on oriented growth of single pyrite crystals with their {001} face on {010} face of a single marcasite crystal. In this case, pyrite crystals have two orientations with respect to the marcasite {010} face. The reason for that lies in non-alignment of 2-fold axes between pyrite in marcasite. Brock and Slater (1978) described another epitactic relationship, where marcasite (101)-twins grow on {001} face of a single pyrite crystal, whereby their (101)-twin planes are oriented perpendicularly with respect to pyrite {001} face. This time the 2-fold axes of both minerals coincide, which results in a single orientation of twinned marcasite on pyrite. In these two cases, the epitactic relationship was ascribed to alignment of Fe-S chains in the structures. Gait and Dumka (1986), and Gait et al. (1990) published the case of single pyrite crystals growth on a cyclic (101)-twinned marcasite. Miklavič et al. (2006) reported on oriented pyrite growth along

the twinning planes of the (101)-twinned marcasite. Orientation of pyrite with respect to marcasite and vice versa is in these two cases the same and results in a single pyrite orientation. Oriented growths of pyrite on arsenopyrite and pyrite on pyrrhotite were described by Zebec (2012). Pyrite is attached with its {001} face to {001} face of arsenopyrite. Non-alignment of 2-fold axes of both minerals again requires two different orientations of pyrite, which is observed on specimens from Trepča. Pyrite is attached with its {001} face to {001} face of pyrrhotite. Octahedral {111} face of pyrite has a chiral trifold symmetry without any mirror plane, whereas the pyrrhotite {001} face has a 6-fold symmetry with 6 mirror planes. For that reason pyrite can have six different orientations on the pyrrhotite that are rotated by 60°, of which four are spatially equivalent. The remaining two are rotated by 180°with respect to each other. Chiral symmetry of the octahedron face requires another two orientations of which one is left- and the other right-handed. In the end, four different orientations remain, of which two are left- and two right-handed, and at the same time rotated by 180°. The outcome is intergrown pyrite with the same surface symmetry as pyrrhotite. Zebec did not specified individual orientations of pyrite on arsenopyrite and pyrrhotite.

Twinned pyrite crystals are rare appearances. The most common are "iron-cross" twins formed by interpenetration of two crystals, rotated by 90° about [110]-axis with respect to each other. The twin acquires the highest cubic $m\overline{3}m$ symmetry. The study of Donnay et al. (1977) found no evidence of impurity metals at the (110)-twin boundaries and that the twinning planes were actually irregular surfaces. The study of Rečnik et al. (2016), on the contrary, showed that a monolayer of Cu atoms was necessary to stabilize the {110} twin structure.

Goldschmidt (1922) published figures (No. 134 and No. 135) of pyrite crystals from Bösingsfelde near Lippe in Germany that are twinned in accordance with two other laws. The first twin type forms by 60°-rotation about the [111]-axis and acquires a hexagonal $6/m$ symmetry. The second type is generated by mirroring in (110) plane with simultaneous 60°-rotation about [111]-axis and yields a twin with the highest trigonal $\overline{3}m$ symmetry. Pabst (1971) reported on pyrite crystals with the unusual form that consist of a central pyrite crystal to which six other are presumably {001}-twinned. The composite crystal resembles a cruciform steacyite twin. In absence of morphological details, an X-ray determination revealed that they were single crystals.

Here, we report on five new twinning laws that were determined on the pyrite crystals from Jean Baptiste section in Lavrion mines.

Methods

In situ sampling of pyrite specimens took place in the period between 2001 and 2020. Specimens for morphological determination with Olympus SZ-11 stereomicroscope were cleaned in an ultrasonic bath filled with a demineralized water. Morphology of single and twinned pyrite crystals was reconstructed using a program SHAPE 7.1.

Camera Sony Alpha III, equipped with LAOWA 25 mm, F 2.8 ultra macro lens was used to photograph specimens, using the focus stacking method.

Three pyrite crystals were chosen for quantitative chemical analysis. All samples were dissolved in hot *aqua regia*. Varian Spectra AA 110 instrument was used to determine Fe, Cu and Zn, and Agilent 7900 ICP-MS instrument was utilized to determine Bi.

Antimony content was analysed by means of electron micro probe analysis (EMPA). The working conditions were set at 20 kV, 10-nA beam current, 2-µm beam size, and peak counting time of 20 s. Nine different crystals within the same polished section were analyzed.

A single crystal of the first generation and a twinned crystal of the second generation, free of visible sfalerite or quartz inclusions, were chosen for a single-crystal X-ray analysis that was conducted on Oxford Xcalibur3 single-crystal X-ray diffractometer equipped with a CCD detector (MoKalpha).

Results

Quantitative chemical analysis

Table 1 summarizes results of iron, copper, zinc, bismuth, and antimony content obtained on samples of tetrahedral pyrite crystals from Jean Baptiste mine section. Iron content in the single crystal of the first generation is close to a theoretical pyrite composition. Contents of other metals are below 0,06 wt%. (001)-twins of the second generation are less pure, which is ascribed to mechanical inclusions of other minerals, especially sfalerite and quartz. Percentage of bismuth is low in all cases and antimony was determined below 0.1 wt % on the (001)-twin of the second generation.

Table 1. Percentage content of metals in pyrite from Jean Baptiste mine section. Sample 1 was a first generation crystal, prepared from the marble, free of microscopically visible sphalerite and quartz inclusions. Samples 2 and 3 were of the second generation and detached from the matrix covered with sphalerite and quartz crystals.

Sample	Fe (wt%)	Cu (wt%)	Zn (wt%)	Bi (wt%)	Sb (wt%)
Single crystal - 1st generation	45,9±0,5	0,052±0,001	0,055±0,001	0,035±0,0010	
(001)-twin - 2nd generation	43,0±0,5	0,113±0,009	0,944±0,009	0,0010±0,0001	
(001)-twin - 2nd generation	43,5±0,5	0,063±0,001	0,049±0,001	0,0007±0,0001	
(001)-twin - 2nd generation					0,06 (0,03 - 0,12)
Theoretical content	46,56				

Morphological analysis

First generation

Pyrite crystals of the first generation are imbedded in marble concordantly with respect to its banding and cover the walls of open veinlets that are perpendicular to the banding (Fig. 2). They are attached to thin crusts of quartz crystals. The smallest pyrite crystals (less than 1 mm) are combinations of strongly striated cube **a**{100} and pentagon dodecahedron **d**{210} faces (Fig. 3A).

Sizes of cube and dodecahedron faces on each single crystal vary greatly, giving the crystals the appearance of deformation. Those imbedded in the marble are fresh and have a strong luster on crystal faces, whereas those from the veins are golden brown due to oxidation. An increase in crystal dimensions is reflected in onset of tetrahedron **t**{110} faces. The larger are the crystals the more developed are the tetrahedrons and the narrower are cube **a**{100} and dodecahedron **d**{210}
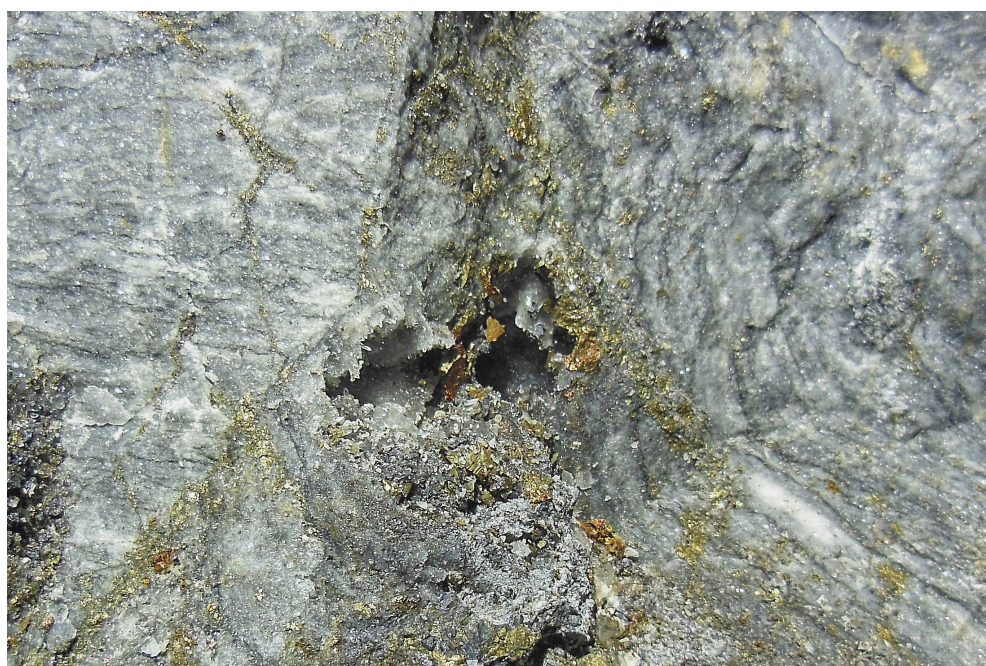
Fig. 2. *In situ* photograph of marble with mineralized ore vein in Jean Baptiste mine section. Pyrite crystals of the first generation are imbedded concordantly with respect to the marble banding and along the veinlets that are oriented more or less perpendicularly to the banding. Pyrite crystals of the second generation with a characteristic rugged pattern grow on quartz and sphalerite crystals in the ore vein. Field of view: 17 cm × 11 cm.
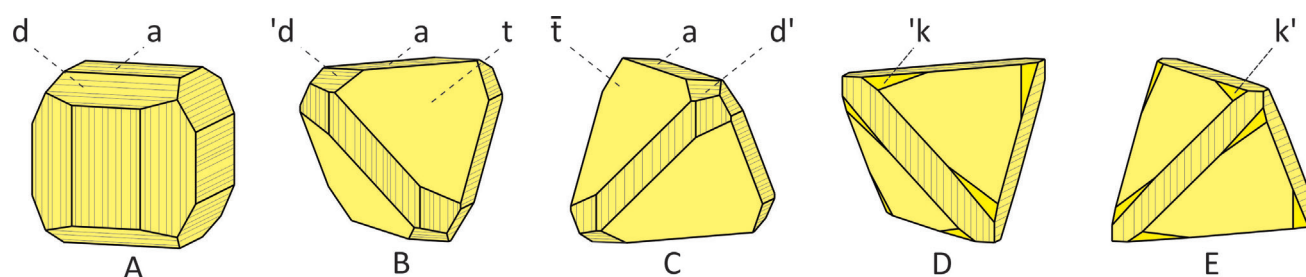
Fig. 3. Crystal morphology of the primary pyrite crystals. Smaller crystals are combinations of cube **a**{100} and pentagon dodecahedron **d**{210} faces. Their alternations are responsible for characteristic striations on crystal faces (A). Larger primary crystals are tetrahedral, and exhibit left- (B) or right-oriented striations on a and d faces (C). This is a reflection of the presence of positive **t**{110} or negative tetrahedron **t̄**{1̄11} faces. Symmetry-defining chiral class-specific forms of left **'k**{11.10.14} (D) and right **k'**{11.10.14} (E) tetrahedral pentagon dodecahedron are frequently present on the crystals.

faces. Striations on cube faces that are the result of alternations of cube and dodecahedrons have a quality of enantiomorphism, which is reflected in crystals with left- or right-handedness. Crystals with positive tetrahedrons **t**{111} are left-handed and vice versa for those with negative $\overline{\textbf{t}}\{\overline{1}11\}$ tetrahedrons (Figs. 3B, 3C and Fig. 4). Consequently, the pentagon dodecahedron **d** gains on specificity by its transformation to class-specific left **'d**{210} or right **d'**{120} tetrahedral pentagon dodecahedron. Handedness of crystals is enhanced by a presence of highly reflective faces of a tetrahedral pentagon dodecahedron **k**{11.10.14}. This class-specific form clearly defines handedness of crystals by its left **'k**{11.10.14} or right **k'**{ $\overline{1}$.10.14} analogue (Figs. 3D and E, and Figs. 4A and B).

Fig. 4. Single pyrite crystals of the first generation on quartz matrix. Calcite crystallized later. Pyrite morphology is defined by tetrahedron t and striated cube a faces. Photographs A and B show left-handed and right-handed crystal, respectively. Note the class-specific faces of the corresponding left **'k**{11.10.14} and right **k'**{11.10.14} tetrahedral pentagon dodecahedron. Both crystals measure one mm on their edges.

Fig. 5. (001)-interpenetration twins of the first pyrite generation. Photograph A shows the twin (one mm in diameter) with a typical reentrant between tetrahedron **t** faces and characteristic striations on cube **a** faces. Better-developed twin on photograph B is 2-fold in all (100) planes. Note the orientations of striations on its cube **a** faces. Twin dimensions: 1.3 mm × 1.3 mm. Faces of dyakis-dodecahedron **k** are present on both crystals in mirror-symmetric positions with respect to (100) planes of symmetry.
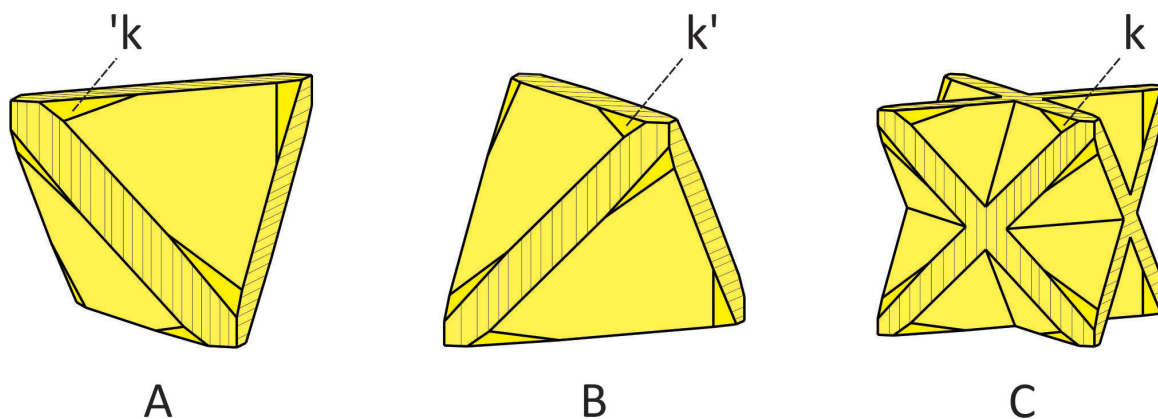
Fig. 6. (001)-interpenetration of single left- (A) and right-handed (B) tetrahedral crystals yields a twin (C). Chiral faces of tetrahedral pentagon dodecahedron forms **'k** and **k'** transform to non-chiral dyakis-dodecahedron **k** (C).
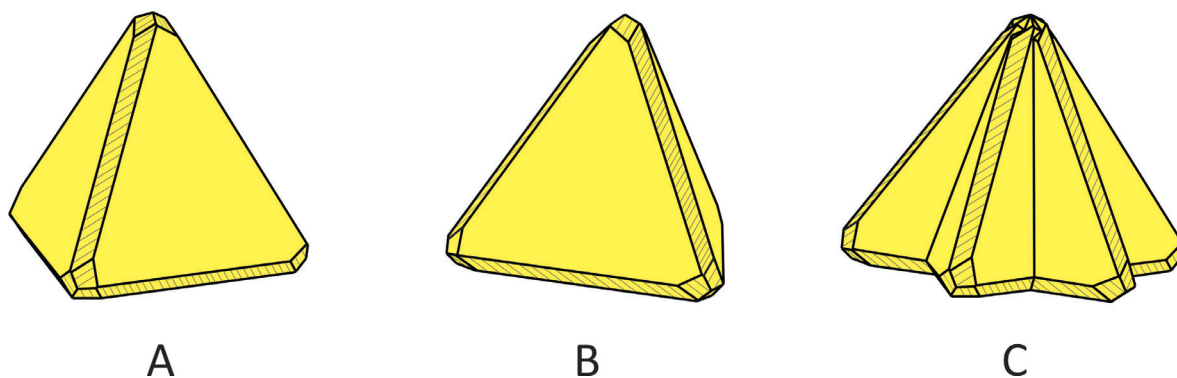
Fig. 7. 6-fold (111)-interpenetration twin (C) is a combination of two left- (shown in the drawing) or two right-handed tetrahedral single crystals, whereby one of them is simultaneously rotated by 60° (B) with respect to the other one (A).

Some of the first pyrite generation crystals are twinned. Two twinning possibilities are noted. The first is twinning by (001)-interpenetration of two tetrahedral crystals of which one is left- and the other right-handed. The resulting twin has deep re-entrants and characteristic orientation of striationson cube **a** faces. Tetrahedral pentagon dodecahedron faces **'k** and **k'** are present in twinning positions, whereby they lose their chiral character and consequently transform to dyakis-dodecahedron **k** (diploid). These twins are rare (Figs. 5 and 6).

The second possibility is interpenetration of two left- or two right-handed tetrahedral crystals about [111]-axis by simultaneous 60°-rotation. The resulting twinned crystal is 6-fold and has a common face (pedion), composed of two tetrahedrons **t**{111} and deep re-entrants between all other tetrahedron faces. The twin retains the
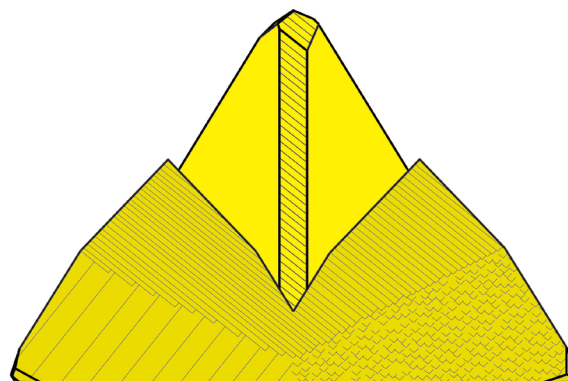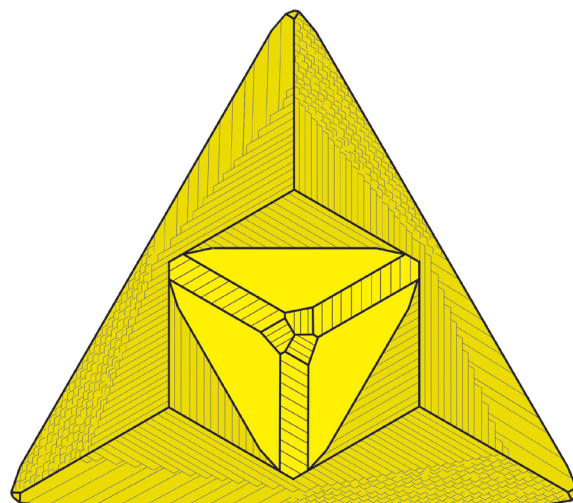
Fig. 8. (111)-interpenetration twins are never theoretically developed. Real crystals exhibit lower 3-fold symmetry, because of the incomplete development of the crystal that surrounds the central one. Drawings above and below show the projection of the right-handed twin along its [111]-twin axis and its projection perpendicularly to the same axis, respectively. Cube a faces are present only on the central crystal. Note the characteristic chiral-specific patterns.

Fig. 9. A group of (111)-interpenetrated twins of the first pyrite generation. Twins in the middle-left and at the top are right-handed and that in the middle-right is left-handed. Heavily striated cube a faces are present on the central crystals only. Surrounding crystals are without them - note their sharp tetrahedral edges. The largest twin measures three mm on its edge.
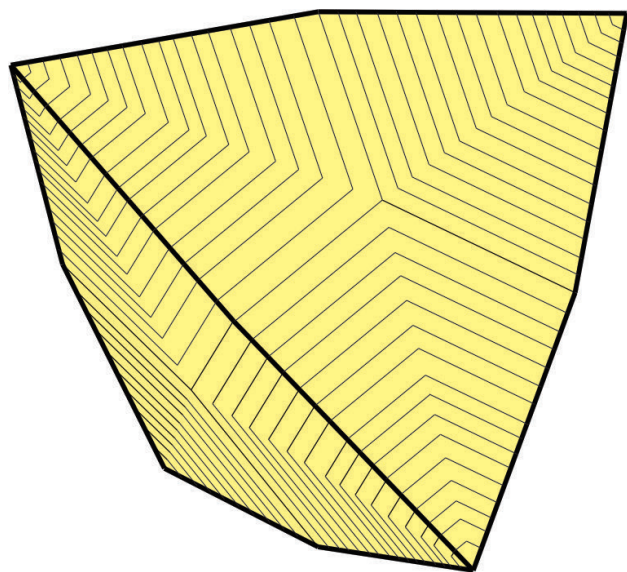
Fig. 10. Pyrite crystals of the second generation have a simple tetrahedral morphology and exhibit characteristic 3-fold mirror symmetric pattern on their faces.

handedness of the interpenetrated single crystals. Faces of tetrahedral pentagon dodecahedron **k** are not present on (111)-twinned crystals. Typical chiral-specific striations appear on tetrahedrons as the result of alternations between tetrahedron **t** and tetrahedral pentagon dodecahedron **d** faces (Figs. 7, 8 and 9). This twinning type may take place on any tetrahedron face, which leads to the formation of more common multiple twins.

Second generation

Pyrite crystals of the second generation have a dull luster and grow only on the walls of the open veins (Fig. 2). If the crystals of the first generation are present, then those of the second generation may overgrow them. They also have a tetrahedral morphology and reach up to 20 mm on their edges. Crystals are sharp-edged due to absence of cube **a**, and dodecahedron **d** faces and lack any traces of handedness. Instead of that,

A   B   C
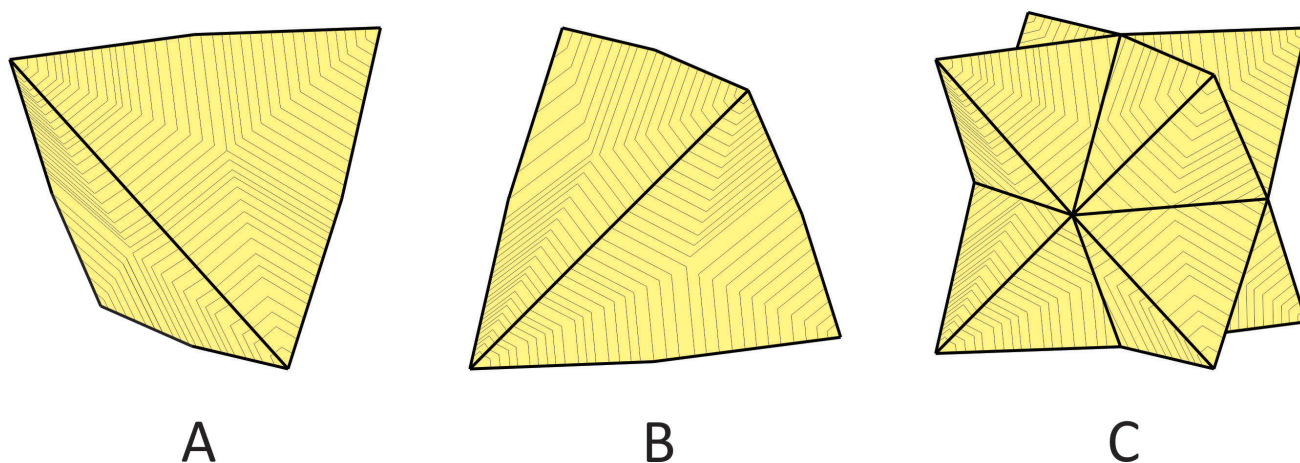
Fig. 12. (001)-interpenetration of two tetrahedral crystals of the second pyrite generation. Crystal B simultaneously rotates by 90° with respect to crystal A. The resulting twin has deep reentrants between tetrahedrons and a mirror-symmetric pattern along all symmetry planes (C).

they exhibit a characteristic mirror-symmetric 3-fold rugged pattern on their tetrahedral faces (Figs. 10 and 11).

Twinned crystals occur in the second generation as well. Again, two twinning possibilities are present. The first is an interpenetration along [001]-axis. Twin is composed of two character-istically patterned tetrahedral crystals and has deep reentrants between them. All patterns are mirror-symmetric in all (100) planes of the twin (Figs. 12 and 13).

The second possibility is an interpenetration along [111]-axis that yields a 6-fold twin that has a common pedion face composed of two tetra-

Fig. 13. (001)-interpenetration twins of the second pyrite generation. Photograph A shows the twin, measuring three mm on its edge, with a typical reentrant between tetrahedron faces. Mirror-symmetric pattern on its faces is present but less-pronounced. Twin photographed along its 4-fold [100]-axis, is presented on photograph B. Its diameter is two mm.
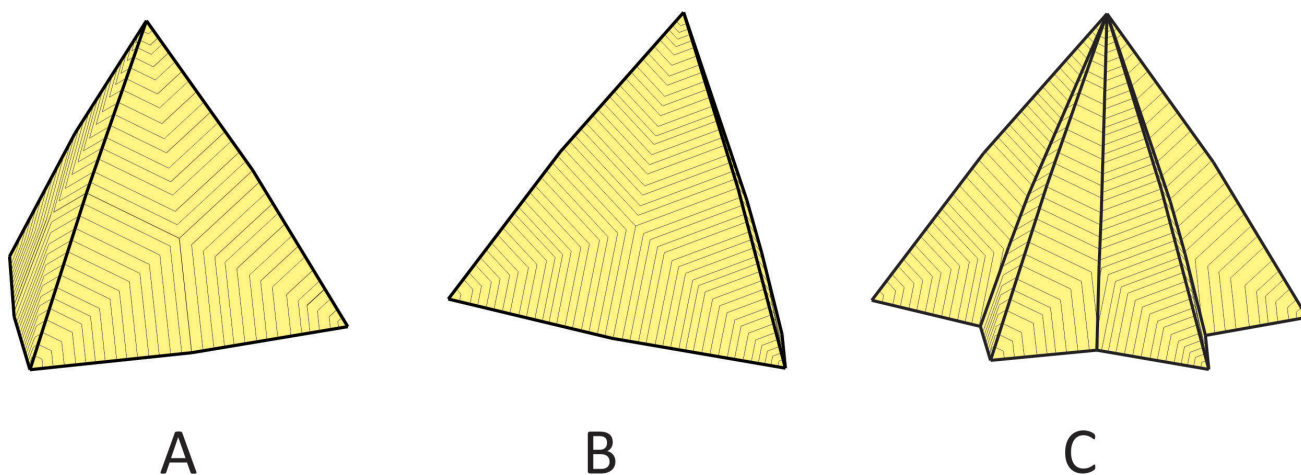
Fig. 14. 6-fold (111)-interpenetration twin (C) is a combination of two tetrahedral crystals, whereby one of them (B) is rotated by 60° with respect to the other one (A). Twin has deep reentrants between tetrahedrons. Note the mirror-symmetric pattern in all symmetry planes of the twin.

hedron faces and with deep reentrants between all other faces. Characteristic mirror-symmetric rugged pattern is present on all faces as well (Figs. 14, 15 and 16). Multiple (111)-interpenetration twinning is very frequent with crystals of this generation (Fig. 16).

Third generation

Pyrite crystals of the third generation do not exceed three mm on their edges. They are oxidized, striated, and composed of cube **a**, pentagon dodecahedron **d,** and exceptionally octahedron **o**{111} faces (Fig. 17). They cover partially or completely pyrite crystals of the second generation. Crystals of the third generation are preferentially attached with their cube faces in parallel with respect to tetrahedron faces of the second-generation crystals, yet in a completely random manner (Fig. 18).

Single-crystal X-ray analysis

All the collected reflections obtained with this structure-discerning method belonged to the common pyrite structure defined by an $m\overline{3}$ point group. No evidence of tetrahedrite inclusions and twin-related reflections were observed neither on the crystal of the first nor on the (001)-twinned crystal of the second generation, after the refinement of the structure to R = 2 %.
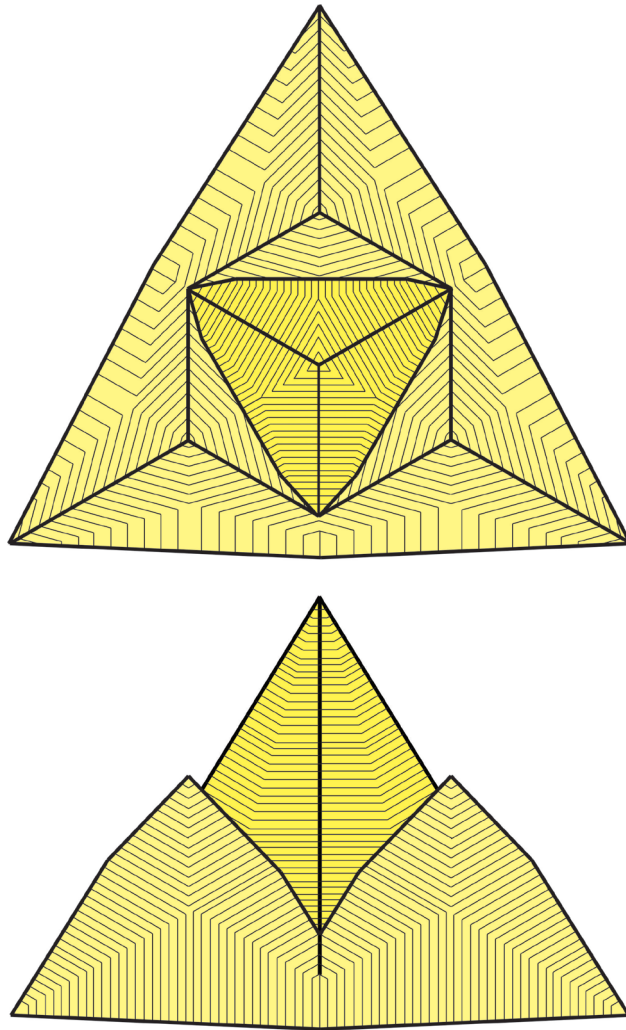
Fig. 15. (111)-interpenetration twins of the second generation are never theoretically developed. Real crystals exhibit lower 3-fold symmetry, because of the incomplete development of the crystal that surrounds the central one. Drawings above and below show the projection of the twin along its [111]-twin axis and its projection perpendicularly to the same axis, respectively. Note the characteristic mirror-symmetric patterns.

Fig. 16. (111)-interpenetration twins of the second pyrite generation. Photograph A shows a typical twin (lower right) with the central crystal and less-developed surrounding crystal. It measures six mm on its lower edge. Twin at the top left shows its pedion face. Crystals are partially covered with thin gypsum crusts. Photograph B shows a multiple (111)-interpenetration twin attached to quartz and sphalerite crystals. A sharp tetrahedral edge of the central crystal protrudes out of the surrounding crystals. Height of the twin is five mm. Characteristic mirror-symmetric rugged pattern is present on all crystals.
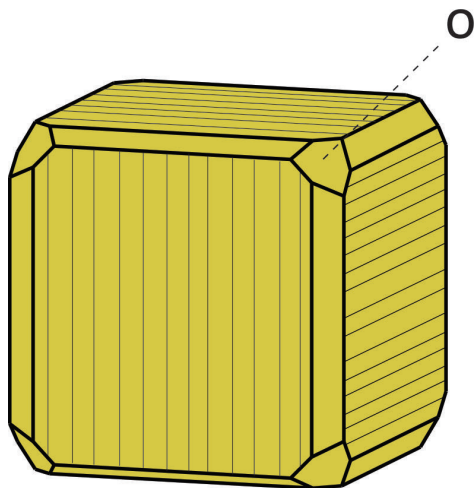
Fig. 17. Pyrite crystals of the third generation have a cubic morphology that is slightly modified by pentagon dodecahedron **d** and octahedron **o**{111} faces.

Fig. 18. Oxidized pyrite crystals of the third generation cover pyrite crystals of the second generation. Note their random orientations on the tetrahedron faces of the secondary generation. The largest crystal measures 11 mm on its tetrahedral edge. Bluish-white coatings are aragonite crystals.

Starting symmetry		Twin symmetry				
		$m\bar{3}$	6	$\bar{4}m3$	$m\bar{3}m$	$6mm$
l-23		*l + r*	*l + l* *r + r*	*l + r*		
r-23						
$\bar{4}m3$						
Twin generation		**1ˢᵗ**		**2ⁿᵈ**		
Interpenetration mode		**(100)**	**(111)**	**(110)**	**(100)**	**(111)**

Fig. 19. Schematic presentation of the observed pyrite crystals from Jean Baptiste section with respect to starting symmetry, generation, and interpenetration mode. Pyrite crystals of the first generation appear as single tetrahedral crystals with left- or right-handed *23* symmetry, as twins with isometric *m$\bar{3}$* symmetry and as simple or multiple twins with left- or right-handed hexagonal *6* symmetry. The second pyrite generation is primarily twinned and has the corresponding *$\bar{4}$m3* symmetry. Crystals of this generation appear as tetrahedrons, as twins with the highest isometric *m$\bar{3}$m* symmetry and as simple or multiple twins with hexagonal *6mm* symmetry.

Discussion

The first to report on pyrite crystals with tetrahedral morphology from Lavrion mine was Mügge in 1895 and 1903. His drawings show left- and right-handed tetrahedral pyrite crystals of the first generation. Crystallographic forms of cube **a**{100}, tetrahedral pentagon dodecahedron **d**{210}, and tetrahedron **t**{111} define the crystal morphology, with chiral-specific striations on **a** faces. The third drawing shows a crystal of the second generation. The apparent low symmetry of the crystals is, in accordance with his opinion, the result of a pyrite pseudomorph after tetrahedrite, whereby he could not detect any traces of tetrahedrite within the crystals, and chemical analysis was negative for copper. Evident tetartohedral symmetry of the pyrite would require its twinning in accordance with "iron cross" in order to adapt to a higher point group of tetrahedrite, which is $\bar{4}m3$, but no signs of such twinning on the primary crystals existed. He concluded therefore, that the evident morphologic tetartohedry could lead to a wrong opinion that the pyrite crystals from this location should have such a low symmetry and stressed that the exact pyrite symmetry was already known at that time beyond any doubt. Mügge (1895) also added that the pyrite crystals appear together with quartz and prismatic arsenopyrite in single and (101)-twinned crystals. The proposed oriented growth of pyrite on tetrahedrite can be understood as a contact of pyrite octahedron {111} face with a tetrahedron {111} face of tetrahedrite. Symmetry of the tetrahedron face is 3-fold with three mirror planes. This symmetry requires left- and right-handed orientation of pyrite. In this way, pyrite acquires the same planar symmetry on its {111} face, i.e. 3-fold with three symmetry planes. Tetrahedrite {111} face, completely overgrown with pyrite in the discussed orientation, could indeed exhibit twinned structure as observed on the second generation of pyrite from Jean Baptiste section. However, it is very likely that the scattered pyrite crystals would only partially cover the tetrahedral faces of real tetrahedrite crystals in two distinctly recognizable chiral orientations, which is not the case here. Oriented growths of pyrite on tetrahedrite or vice versa are not known.

Since then, no new works on the subject, and no new material had appeared until 2001, when a group of researchers from Athens rediscovered the location and collected new specimens (Voudouris et al., 2004). A preliminary SEM analysis was performed to determine which mineral the tetrahedral crystals belonged to. It turned out that they were pure pyrite without indication for replacement of another mineral.

It is clear that Mügge described the primary crystals from exactly the same location, because the tetrahedral pyrite crystals from the new find have the same morphology and come together with arsenopyrite in single and (101)-twinned crystals. Besides that, no other location with tetrahedral pyrite crystals has ever been encountered in Lavrion mines. It has to be stressed that the pyrite crystals of the first generation exhibit the evident morphological lowermost cubic symmetry *23*. ICP-MS analysis of primary crystals confirmed the purity of the first-generation pyrite crystals with respect to their Cu, Zn, and Bi content. EMPA analysis of the second-generation pyrite crystals showed the comparably low antimony content (see Table 1). Single-crystal X-ray analysis excluded tetrahedrite inclusions in single and in twinned crystals.

Discovery of different interpenetration twin types on the new material sheds a completely new light on the trivial symmetry of the tetrahedral pyrite crystals at Jean Baptiste location. Formation of (001)-interpenetration twins, exhibiting a cubic $m\bar{3}$ symmetry as presented in Figure 5, is not possible unless the starting symmetry is the lowermost isometric *23* (tetartohedry). Figure 6 shows the formation of such a twin. (111)-interpenetration twins are another proof of lower primary symmetry, because they are chiral and retain the handedness of the twinned single crystals, which is only possible if the starting symmetry is *23*. The resulting twins with symmetry *6* are for that reason either left- or right-handed (see Fig. 7). Real twinned crystals of this type exhibit lower, but evidently chiral *3* symmetry as the outcome of the incomplete interpenetration (Figs. 8 and 9).

All tetrahedral pyrite crystals of the second generation have a characteristic 3-fold mirror-symmetric pattern on tetrahedron faces. This fact reflects a higher symmetry, which is the result of (110)-interpenetration in which two tetrahedral crystals of the opposite handedness interpenetrate (Fig. 19).

All pyrite crystals of the second generation are therefore twins with $\bar{4}m3$ symmetry, which enables further twinning by (001)-interpenetration yielding a twin with the highest cubic $m\bar{3}m$ symmetry. Twins of this type exhibit sharp tetrahedral edges and characteristic rugged pattern on their faces that is mirror-symmetric along all (100) and (110) planes of symmetry (Figs. 12 and 13).

The highest twin symmetry appears when two crystals of the second pyrite generation are (111)-interpenetrated by simultaneous 60°-rotation about the [111]-axis. The resulting twin has a hemimorph *6mm* symmetry with a characteristic pattern on all tetrahedral faces that is mirror symmetric along six mirror planes that are parallel to the twin's main 6-fold axis (Fig. 14). Real crystals exhibit lower symmetry due to incomplete interpenetration (Figs. 15 and 16A). Multiple twinning of this type is frequent (Fig. 16B). Figure 19 shows a schematic presentation of all described twinning possibilities.

Pyrite crystals of the third generation are cubes that are slightly moderated by pentagon dodecahedron **d** and octahedron **o**{111} faces on cube corners. There are no twinning signs on them, which confirms their trivial $m\overline{3}$ symmetry.

The cubic $m\overline{3}$ symmetry of the first-generation single crystals as well as of the (110)-twinned crystals of the second generation derives from the findings of the single-crystal X-ray analysis conducted on them. It is therefore evident, that the results of morphological and structural analysis do not match. It is not the aim of this study to specify the environmental and structural details leading to the formation of the observed twins. To explain this discrepancy, we may only propose that the pyrite crystals of the first generation crystallized under conditions that favored their initial low isometric *23* symmetry, and consequently the formation of tetrahedral crystals and twins. Crystallization conditions might change in the course of time and the initial symmetries (crystal structures) of all single and twinned crystals of the first and the second generation transformed to structures with higher $m\overline{3}$ symmetry, whereas their morphologies remained unchanged.

The other explanation might consider a possible insufficient specificity of the single-crystal X-ray analysis. Namely, pyrite trivial $m\overline{3}$ point group ranks to a group of centrosymmetric Laue classes. Two crystals measured in this study, on the contrary, belong to morphologically evident non-centrosymmetric *23* and $\overline{4}m3$ point groups that may mimic the centrosymmetric $m\overline{3}$ one if a resonant scattering (anomalous dispersion) was negligible or not detected.

Future work on this topic should therefore go into direction of determining conditions during the formation and growth of three pyrite generations, which would include the determination of physico-chemical growth parameters, fluid inclusions in crystal paragenesis and into the optimization and refinement of the single-crystal X-ray analysis.

References

Berger, A., Schneider, D. A., Grasemann, B. & Stockli, D. 2013: Footwall mineralization during Late Miocene extension along the West Cycladic Detachment System, Lavrion, Greece. Terra Nova, 25: 181-191.

Bonsall, T. A., Spry, P. G., Voudouris, P., Tombros, S., Seymour, K. & Melfos, V. 2011: The Geochemistry of Carbonate Replacement Pb-Zn-Ag Mineralization in the Lavrion District, Attica, Greece, Fluid Inclusion, Stable Isotope, and Rare Earth Element Studies. Econ. Geol., 106: 619-651.

Brock, K. J. & Slater L.D. 1978: Epitaxial marcasite on pyrite from Rensselaer, Indiana. American Mineralogist, 63: 210-212.

Conophagos, C. 1980: The Lavrion and the ancient Greek techniques for silver production. Athens, Ekdotiki Athinion: 458 p.

Gait, R. I. & Dumka, D. 1986: Morphology of pyrite from the Nanisivik mine, Baffin Island, Northwest territories. Canadian Mineralogist, 24/4: 685–688.

Gait, R. I., Robinson, G. V., Bailey, K. & Dumka, D. 1990: Minerals of the Nanisvik Mine, Baffin Island, Northwest Territories. Mineralogical Record, 21/6: 515-534.

Goldschmidt, V. M. 1922: Atlas Der Krystallformen, Bd. VI. Verlag Winters, Heidelberg.

Marinos, G. & Petrascheck, W. E. 1956: Lavrion: geological and geophysical research. Inst. Geol. Subsurf. Res. 4: 246.

Miklavič, B., Žorž, M. & Schmidt, G. 2006: Markazit in pirit izpod Prisojnika. In monograph: Mineralna bogastva Slovenije. Scopolia, Suppl. 3: 439-443.

Morin, D. & Photiades, A. 2012: L'exploitation des gisements métallifères profonds dans l'Antiquité. Les mines du Laurion (Grèce).

Eckart Olshausen/Vera Sauer (Hg.) Die Schätze der Erde – Natürliche Ressourcen in der antiken Welt. Stuttgarter Kolloquium zur Historischen. Geographie des Altertums 10, 2008. Geographica Historica 28. Franz Steiner Verlag Stuttgart 2012: 28-335. CD-Rom Illustrations. ISBN 978-3-515-10143-1.

Mügge, O. 1895: Regelmässige Verwachsung von Pyrit mit Fahlerz in Pseudomorhosen nach letzteren. Neues Jahrbuch für Mineralogie, Geologie und Palaentologie, I. Band: 103-105.

Mügge, O. 1903: Die regelmässige Verwachsungen von Mineralien verschiedener Art. Neues Jahrbuch für Mineralogie, Geologije und Palaentologie, XVI. Beilage – Band: 340-341.

Pabst, A. 1971: Pyrite of unusual habit simulating twinning from the Green River Formation of Wyoming. American Mineralogist, 56/1-2: 133-145.

Rečnik, A., Zavašnik, J., Jin, L., Čobić, A. & Daneu, N. 2016: On the origin of "iron-cross" twins of pyrite from Mt. Katarina, Slovenia. Mineralogical Magazine, 80/6: 937-948. https://doi.org/10.1180/minmag.2016.080.073

Richards, R. P., Clopton, E. L. & Jaszczak, J. A. 1995: Pyrite and marcasite intergrowths from northern Illinois. Mineralogical Record, 26/2: 129-138.

Scheffer, C., Tarantola, A., Vanderhaeghe, O., Voudouris, P., Rigaudier, T., Photiadis, A., Morin, D. & Alloucherie, A. 2017: The Lavrion Pb-Zn-Fe-Cu-Ag detachement-related district (Attica, Greece): Structural control on hydrothermal flow and element transfer-deposition. Tectonophysics, 717/16: 607-627. https://doi.org/10.1016/j.tecto.2017.06.029

Scheffer, C., Tarantola, A., Vanderhaeghe, O., Voudouris, P., Spry, P.G., Rigaudier, T. & Photiades, A. 2019: The Lavrion Pb-Zn-Ag-rich Vein and Breccia Detachment-Related Deposits (Greece): Involvement of Evaporated Seawater and Meteoric Fluids during Post-Orogenic Exhumation. Economic Geology, 114/7: 1415-1442. https://doi.org/10.5382/econgeo.4670

Skarpelis, N. 2007: The Lavrion deposit (SE Attica, Greece): geology, mineralogy and minor elements chemistry. Neues Jahrbuch für Mineralogie Abhandlungen, 183/3: 227-249. https://doi.org/10.1127/0077-7757/2007/0067

Voudouris, P., Tsolakos, A., Papanikitas, A. & Solomos, Ch. 2004: Nicht nur Micromounts Neufunde aus Lavrion. Lapis, 4: 13-15.

Voudouris, P., Melfos, V., Spry, P.G., Bonsall, T., Tarkian, M. & Solomos, Ch. 2008: Carbonate-replacement Pb-Zn-Ag±Au mineralization in the Kamariza area, Lavrion, Greece: Mineralogy and thermochemical conditions of formation. Mineral. Petrol., 94/1-2: 85-106. https://doi.org/10.1007/s00710-008-0007-4

Voudouris, P., Melfos, V., Mavrogonatos, C., Photiades, A., Moraiti, E., Rieck, B., Kolitsch, U., Tarantola, A., Scheffer, C., Morin, D., Vanderhaeghe, O., Spry, P.G., Ross, J., Soukis, K., Vaxevanopoulos, M., Pekov, I.V., Chukanov, N.V., Magganas, A., Kati, M., Katerinopoulos, A. & Zaimis, S. 2021: The Lavrion Mines: A Unique Site of Geological and Mineralogical Heritage. Minerals, 11/1: 76. https://doi.org/10.3390/min11010076

Zebec, V. 2012: Trepča/Stari trg, Zagreb: 415 p.

Žorž, M. 2019: The Symmetry System, 2nd edition, Ljubljana: 212 p.